Materials Advances

ROYAL SOCIETY OF CHEMISTRY

PAPER

View Article Online
View Journal | View Issue

Cite this: *Mater. Adv.*, 2024, 5, 282

Structuring biogenic synthesis of rare phase $LaMn_2O_5$ using the *Bauhinia variegata* (Kachnar) flower extract for highly sensitive, long range electrochemical detection of bisphenol-A, an endocrine disruptor†

Ankur Srivastava, Kshitij RB Singh, Mrituanjay D. Pandey * and Jay Singh *

This work presents the *in situ* biogenic synthesis of rare phase nanostructure $LaMn_2O_5$ by the hydrothermal method, using the *Bauhinia variegata* (Kachnar) extract to prevent the discharge of hazardous and toxic waste elements into the environment. In this study, the compound exhibits strong Mn-3p and O-2p interactions, closely associated with vacant La-4f orbitals resulting in strong covalent bonding. Moreover, the synergetic effect of the f–d block metals effectively facilitates electron transfer. In this work, biologically derived, rare phase $LaMn_2O_5$ was also fabricated as a bioelectrode and developed into an electrochemical sensor. The estimated biosensor was assessed across a wide range of analyte concentrations for detecting the plastic monomer and endocrine disruptor bisphenol-A (BPA). A three-step linear response was observed, spanning from 0.001 μM to 0.1 μM, 1.0 μM to 40 μM and 40 μM to 1000.0 μM with a limit of detection (LOD) value of 2.85×10^{-3} μM and negligible interference. The sensitivity was obtained to be 3.67 mA μM^{-1} cm^{-2}. Cyclic voltammetry (CV), pH, and scan rate studies were also performed for the prepared nanomaterials. From the scan rate study, the diffusion coefficient (D), charge transfer rate (K_s), and surface concentration (γ) were calculated which were found to be appreciable. The synthesized rare phase nanostructure $LaMn_2O_5$ exhibited a response time of 30 seconds, 60 days long stability, and 13 times reusability. This study reveals the biogenic synthesis of rare phase nanostructure $LaMn_2O_5$. This innovative method has the potential to harness natural resources for the synthesis of distinct nanomaterials. The rare phase nanostructure $LaMn_2O_5$ appears to be highly susceptible, in the long-range detection of BPA.

Received 2nd October 2023,
Accepted 18th November 2023

DOI: 10.1039/d3ma00790a

rsc.li/materials-advances

1. Introduction

Manganese is the second most abundant transition metal on the Earth's crust and has been utilized as a vital element in steel production, glass making, and desulfurization since the mid-19th century. It is an essential micronutrient for the survival of many organisms living on the Earth's surface.[1,2] Moreover, the potentials of the manganese oxides have been utilized in various field like, optical, electrical, and as a contrast agent for magnetic resonance imaging.[3] The other derivatives of manganese oxides like Mn_2O_3 and Mn_3O_4 have been employed in supercapacitors due to their physiochemical stability, non-toxic nature, and flexibility.[4] Manganese oxides have also been utilized in electrochemical biosensing[5] and energy storage.[6]

However, the combination of lanthanides has been reported with the s-block and d-block elements, such as potassium[7] and gold metal,[8] and fabricated for the electrochemical detection of dopamine. Previous literature also explored the use of lanthanide–manganese-based nanomaterials in various fields. Nickel and iron-doped lanthanum manganese oxide has been utilized for biohydrogen production[9] and lanthanum has been utilized with Mn-ferrite for magnetic study.[10] Tao Chen *et al.* reported carbon $SmMn_2O_5$ nanomaterials for the catalytic oxidation of nitric oxide[11] and Z. Y. Zhao *et al.* reported dysprosium-based manganese oxide, $DyMn_2O_5$, for electric polarization, magnetic field, and temperature function purposes.[12] Pressure-dependent X-ray diffraction studies have been carried out for RMn_2O_5 (R = Gd, Pr, and Sm).[13] In this way Yan Chen *et al.* reported the study of the magnetic properties of RMn_2O_5 (R = La, Pr, Nd, Tb, Bi).[14] Moreover, lanthanum-doped manganese

Department of Chemistry, Institute of Science, Banaras Hindu University, Varanasi-221005, Uttar Pradesh, India. E-mail: mdpandey.chem@bhu.ac.in, jaysingh.chem@bhu.ac.in; Tel: +91-9871766453

† Electronic supplementary information (ESI) available. See DOI: https://doi.org/10.1039/d3ma00790a

dioxide has shown potential for breast cancer therapy[15] but there are limited research articles available for biosensing applications based on this nanostructure. However, if we focused on the synthesis procedure, nonetheless, most of the previous works have employed chemical routes which produce toxic and hazardous chemicals and create unhealthy environments. A biogenic route is a safe way to avoid toxic and harmful chemicals, reagents,[16] capping agents, and surfactants.[17] In this way the we found that *Bauhinia variegata* (Kachnar) contains 24 types of terpenoids and sesquiterpenoids such as α-pinene, β-pinene, δ-cadinine and γ-elemene, which can be utilized in the reaction as a reducing agent and capping agent.[18]

This work reports the synthesis of biogenic rare-phase nanostructure $LaMn_2O_5$ using the *in situ* hydrothermal method, where the *Bauhinia variegata* (Kachnar) extract was employed as a reducing agent, capping agent, and surfactant. To the best of our knowledge and based on reported literature, no research work is available on the one-step biogenic synthesis of $LaMn_2O_5$ materials and its enzymatic fabrication in the form of a Tyr/$LaMn_2O_5$/ITO bioelectrode. This electrode functions as a biosensor for the long-range detection of endocrine disruptor bisphenol-A (2,2-bis(4-hydroxyphenyl)propane) (BPA), which was first reported in 1891 by Dianin,[19] responsible for the growth of cancerous cells in mammals. The proposed electrochemical biosensor serves as an optimistic window for the fabrication of a low-cost, easy-to-handle, efficient, and sensitive electrode for BPA detection. The highly selective electrochemical estimation was carried out for the long-range detection of BPA, in the detection range of 0.001–1000 μM including three linear range intervals. Appreciable linear regression coefficients (R^2) were obtained (0.9757, 0.9923, and 0.9781). The sensor was found to have 60 days long stability, 30 seconds quick response time, high sensitivity, and an effective limit of detection (LOD) value, which has great potential to be developed as an electrochemical device in the future.

2. Experimental

2.1. Materials and method

Potassium hexacyanoferrate(III) ($K_3[Fe(CN)_6$]; MW: 329.25 g mol^{-1}; product cat no: 1.93667.0521), potassium hexacyanoferrate(II) trihydrate ($K_4[Fe(CN)_6]\cdot 3H_2O$; MW: 422.39 g mol^{-1}; product cat no. 1.93686.0521), sodium chloride (NaCl; MW: 58.44 g mol^{-1}; product cat no. S9888), ammonia liquor (NH_3; MW: 17.03 g mol^{-1}; CAS no. Q16225) were obtained from Qualigens, Thermo Fisher Scientific. Whatman filter paper grade-1 was obtained from Sigma-Aldrich. Monosodium phosphate (NaH_2PO_4; MW: 119.98 g mol^{-1}; CAS no. 7558-80-7) and disodium phosphate ($Na_2HPO_4\cdot H_2O$; MW: 177.99 g mol^{-1}; CAS no. 10028-24-7)were procured from Himedia. Lanthanum nitrate hexahydrate was procured from SRL and manganese nitrate tetrahydrate from Sigma Aldrich. Bisphenol-A ($C_{15}H_{16}O_2$; MW: 228.29 g mol^{-1}; CAS no. 80-05-7) was obtained from Sigma-Aldrich. Uric acid ($C_5H_4N_4O_3$; MW: 168.1103 g mol^{-1}; CAS no. 69-93-2) from Sigma Aldrich. Urea (CON_2H_4; MW: 60.06 g mol^{-1}; CAS no. 57-13-6), DL-lactic acid ($C_3H_6O_3$; MW: 90.08 g mol^{-1}, CAS no. 50-21-5) was from Merck. Glutamic acid ($C_5H_9NO_4$; MW: 147.13 g mol^{-1}; CAS no. 56-86-0) was from Sigma Aldrich. Glucose ($C_6H_{12}O_6$; MW: 180.15 g mol^{-1}; CAS no. 50-99-7) was from SDFCL. L-Ascorbic acid ($C_6H_8O_6$; MW: 176.12 g mol^{-1}; CAS no. 50-81-7) was from Sigma Aldrich. Resorcinol ($C_6H_4(OH)_2$; MW: 110.11 g mol^{-1}; CAS no. 108-46-3) was from Fisher Scientific. 2-Aminophenol (C_6H_7NO; MW: 109.13 g mol^{-1}; CAS no. 95-55-6), 4-aminophenol (MW: 109.13 g mol^{-1}; CAS no. 123-30-8) were from Avra Synthesis Pvt. Ltd. Hydroquinone ($C_6H_4(OH)_2$; MW: 110.11 g mol^{-1}: CAS no. 123-31-9) was from Fisher Scientific. 2-Nitrophenol ($C_6H_5NO_3$; MW: 139.11 g mol^{-1}; CAS no. 88-75-5) was from Sigma-Aldrich. *Bauhinia variegata* (Kachnar) was obtained from the garden of the department. All the chemicals used in the experiments were of analytical grade and used without further purification. The ITO sheets having a surface resistivity of 20 Ω sq^{-1} were obtained from Sigma-Aldrich. Hydrogen peroxide (MW: 34 $nmol^{-1}$; product cat no. 1.93007.0521). Milli-Q water (18 U resistivity; Millipore, USA) was used in all the experimental works.

2.2. Preparation of the *Bauhinia variegata* (Kachnar) extract

To prepare the Kachnar extract, 20 mg of flowers were thoroughly washed with double distilled water and then air dried for two days. The dried flowers were added to 180 mL of water, maintaining the ratio of 10 : 90 in a total volume of 200 mL of water. The mixture was boiled at 60 °C for 30 minutes and subsequently filtered using Whatman filter paper. Finally, the filtered solution was allowed to cool for approximately 35 minutes and stored for further reaction.

2.3. Preparation of the rare phase $LaMn_2O_5$ nanostructure

To synthesize the rare phase nanostructure $LaMn_2O_5$ a 20 mL solution of 0.1 M $La(NO_3)\cdot 6H_2O$ (pH = 5) was mixed with a 20 mL solution of 0.05 M $Mn(SO_4)$. H_2O (pH = 6). Further, a 5 M NaOH solution was added to make the solution basic and the pH was adjusted to approximately 12. Subsequently, 20 mL of the previously prepared *Bauhinia variegata* (Kachnar) extract was added to the above solution, transferred to the Teflon hydrothermal autoclave, placed inside the muffle furnace, and heated to 180 °C for 24 hours. After the reaction was complete, it was allowed to cool and the compound was washed 3–4 times with Milli-Q water and a 20% water–ethanol mixture. The compound was collected by centrifugation at 10 000 rpm and dried in a vacuum oven at 60 °C until further characterization. The reaction involved in this process is shown in eqn (1):

$$\mathrm{La(NO_3)\cdot 6H_2O + 3NaOH \xrightarrow{RT} La(OH)_3 + 3NaNO_3 + 6H_2O}$$

$$\mathrm{2Mn(NO_3)\cdot 3H_2O + 4NaOH \xrightarrow{RT} 2Mn(OH)_2 + 2NaNO_3 + 3H_2O}$$

$$\mathrm{La(OH)_3 + 2Mn(OH)_2 \xrightarrow[18h]{180^\circ C} LaMn_2O_5} \quad (1)$$

2.4. Fabrication of the Tyr/$LaMn_2O_5$/ITO bioelectrode

The prepared electrode was fabricated using the drop-casting method and converted into a bioelectrode. To do this, a solution of tyrosinase enzyme from Agaricus bisporus with an

activity of 1000 U mg^{-1} was used. The solution had a concentration of 1 mg mL^{-1} of PBS solution, pH 6.5. Further, 10 μL of the tyrosinase enzyme solution was allowed to uniformly spread onto the ITO surface (surface area of 0.25 cm^2), which was then placed at 4 °Covernight to ensure proper binding of the enzyme on the ITO surface. Fig. 1 shows a schematic representation of the preparation of rare phase nanostructure $LaMn_2O_5$.

3. Results and discussion

3.1. Structural characterization

3.1.1. Powder XRD. The biologically derived rare phase nanostructure $LaMn_2O_5$ was analyzed by powder X-ray diffraction (XRD) to determine its phase and average crystallite size. The experiment was conducted using a Bruker D8 Advance X-ray diffractometer with Cu-K radiation at a wavelength of 1.5406 Å. The scan rate was 2 degrees per minute and 2θ angles ranged from 10° to 90° with λ = 1.5406 Å. The results correspond to JCPDS card no. 88-0084 and the *hkl* value for the most intense peak was found at 201, 121, and 211 with *d*-spacing values of 3.18, 3.15, and 2.99 respectively (Fig. 2(A)). The material was found to have an orthorhombic structure, with a primitive type lattice with lattice parameters a = 7.68, b = 8.70, and c = 5.71. Moreover, Zhen Chen in 2012 reported the crystalline arrangements of this type of compound where each unit cell consists of four formula units, with $Mn^{3+}O^5$ pyramids and $Mn^{4+}O^6$ octahedra.[20] The compound was found to be crystalline and the average crystallite size of the compound was calculated from the Scherrer equation[21] to be 14.75 nm (eqn (2)):

$$D = K\lambda/\beta\cos\theta \quad (2)$$

where D is the average crystallite size, K is the Scherrer constant (0.9), λ (1.5406 Å) is the wavelength applied for the diffraction, and β is the full width at half maximum (rad).

3.1.2. FT-IR analysis. The presence of a significant functional group was identified by FT-IR spectroscopy using a Nicolet iS5-Thermo Fisher Scientific spectrophotometer over the range of 400–4000 cm^{-1}. This type of compound shows a strong correlation effect, indicating a strong bonding interaction with atoms of functional groups present in the compound.[20] The FT-IR spectra of the prepared compound, shown in Fig. 2B, exhibited a strong peak at 3430 cm^{-1} corresponding to the N–H bond and a peak at 2918 cm^{-1} for the C–H stretching bond. The most characteristic peaks for Mn–O[22] and La–O bonds[23] were obtained at 562 and 638 cm^{-1} respectively which merged, whereas the peaks obtained at 746 cm^{-1} correspond to the Mn–O–Mn bond, closely related to a previously reported study.[24] The rare phase material was synthesized from the Kachnar extract which contains hydrocarbons with carbonyl groups. As a result, the peaks obtained at 1724, 1280, and 1087 cm^{-1} were found to be of carbonyl stretching, and C–C and C–O–C bonds[22] respectively, obtained from the Kachnar extract which has a variety of functional groups.

3.1.3. UV and fluorescence study. The absorption spectra of the compound were obtained using an Agilent Cary 60 UV-Vis spectrophotometer, in the 200–800 nm wavelength range, with water as a dispersing medium. Two clear sharp absorption peaks were observed at 229 and 276 cm^{-1}. These peaks were ascribed to the π–π* and π–nb* electronic transitions present in the Mn═O, Mn–O–Mn, and La–O bonds (Fig. 2(C)). The UV graph plot between $(\alpha h\nu)^2$ and $E = hc/\lambda$ revealed two binding energy values at 4.25 and 4.70 eV, as shown in Fig. 2(C, inset). These values indicate the presence of two different bonding environments in $LaMn_2O_5$. Additionally, to reveal the fluorescence properties of the compound emission spectra were recorded using a Horriba Fluoromax spectrophotometer. A strong peak observed at 365 nm suggests that the rare phase $LaMn_2O_5$ compound is highly fluorescent as depicted in Fig. 2(D).

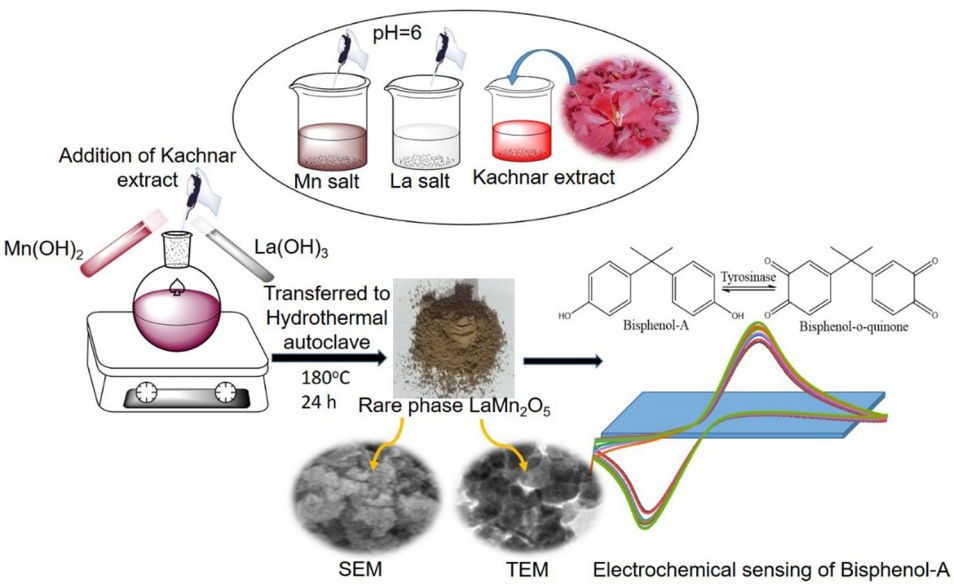

Fig. 1 Schematic representation of the preparation of the rare phase $LaMn_2O_5$ nanostructure.

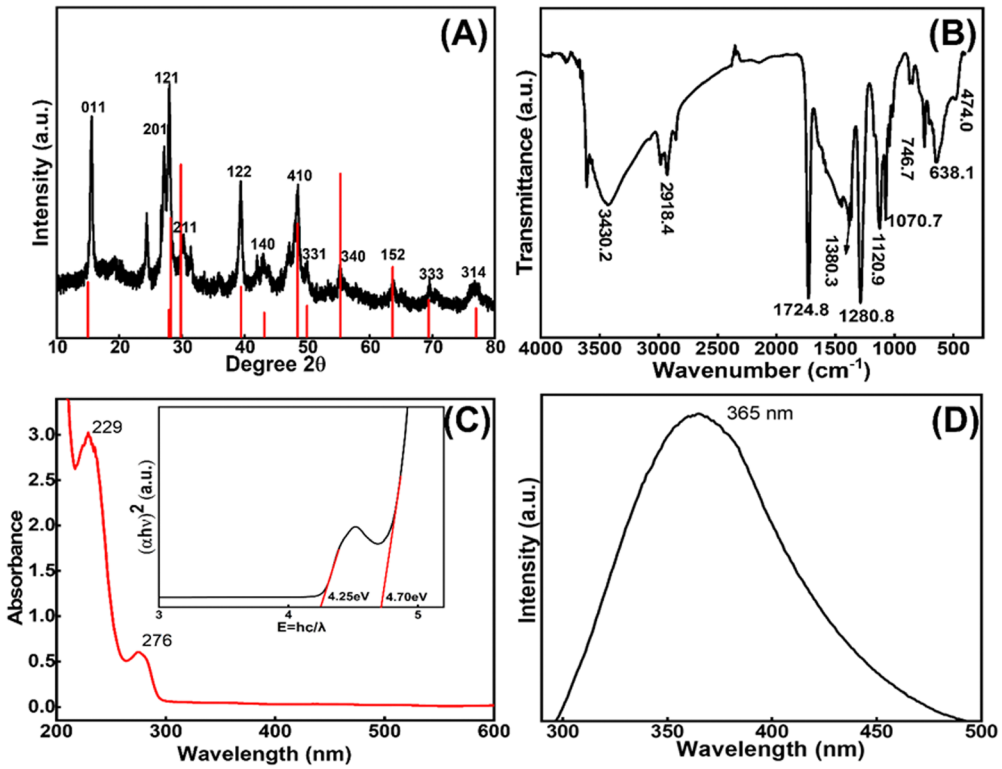

Fig. 2 (A) X-ray diffraction crystallography of $LaMn_2O_5$, (B) FT-IR spectra of rare phase nanostructure $LaMn_2O_5$, (C) UV-visible spectra of $LaMn_2O_5$ (inset: the Touc plot of the UV graph representing the binding energy of $LaMn_2O_5$) and (D) Photoluminescence spectra of rare phase nanostructure $LaMn_2O_5$.

3.1.4. XPS analysis. XPS was performed using a PHI 5000 Versa Probe III, with Al Kα radiation ($h\nu$ = 1486.6 eV). The XPS Al Kα X-ray spot size was adjustable from 10 μM to 200 μM and scanning XPS with up to 1.4 mm. The chemical state and chemical composition of the elements present in the prepared material were revealed by XPS analysis and deconvolution of the spectra was carried out using XPS-peak-41 software. The survey spectra of $LaMn_2O_5$ clearly represented all the corresponding peaks present in the prepared materials, as shown in Fig. 3(A). The presence of the La 3d peak in $LaMn_2O_5$ apparently indicates that La was successfully doped into the nanostructure. The deconvoluted spectrum of La 3d revealed a doublet peak at 849.8 and 836.6 eV, resembling La $3d_{3/2}$ and La $3d_{5/2}$ for La^{3+}, as shown in Fig. 3(B). The appearance of two peaks at 651.4 and 639.7 eV for the Mn 2p spectra of $LaMn_2O_5$ correspond to Mn $2p_{3/2}$ and Mn $2p_{5/2}$,[25] respectively (Fig. 3(C)). Moreover, the O 1s core level spectrum was observed to distinguish the oxygen state, as shown in Fig. 3(D). The peak obtained consists of only one binding energy at 529.3 eV indicating a single type of bonding in the compound, which was ascribed to the surface lattice oxygen.[26]

3.2. Morphological analysis

3.2.1. Atomic force microscopy analysis. The three-dimensional analysis of surface morphology was performed using atomic force microscopy (AFM), which is unique for *z*-axis analysis along two (*x* and *y*) dimensions. It was recorded using NEXT and NT-MDT instruments. To perform AFM, a sample was prepared on an ITO glass surface using an electrophoretic deposition technique. AFM was performed with and without enzymatic deposition to analyse the morphological changes after enzyme deposition. The root mean square roughness (Rms-R_q), average roughness (R_a), and maximum area peak height were determined for $LaMn_2O_5$/ITO and Tyr/La_2MnO_5/ITO bioelectrodes, as shown in Table 1.

It was observed that the Rms-R_q, R_a and maximum area peak height values were found to be higher for enzyme deposited compounds as compared to compounds without enzyme deposition. This is because the enzymatic functional group may provide higher roughness and height, which is an indication of appreciable interaction between the materials and enzymes (Fig. 4(A and B)). Moreover, the average roughness (R_a) was found to be about 12 times higher than that of the enzymatic compound, indicating an increased surface area of the electrode. Moreover, the morphological arrangement for $LaMn_2O_5$/ITO was found to be uniform with spherical-shaped particles. The morphological arrangements for the Tyr/La_2MnO_5/ITO bioelectrode are shown in Fig. 4(C and D).

3.2.2. SEM, TEM, HR-TEM and EDAX. The surface morphology was analysed using SEM(Carl Zeiss, EVO-18, Research Model, Germany). SEM images of the rare phase nanostructure $LaMn_2O_5$ demonstrated some cloudy and spherical morphological arrangements, as shown in Fig. 5(A and B). It apparently has surface folds and a layered structure in which the lanthanum and manganese oxide nanoparticles are uniformly intermixed with each other. The elemental composition was determined from the

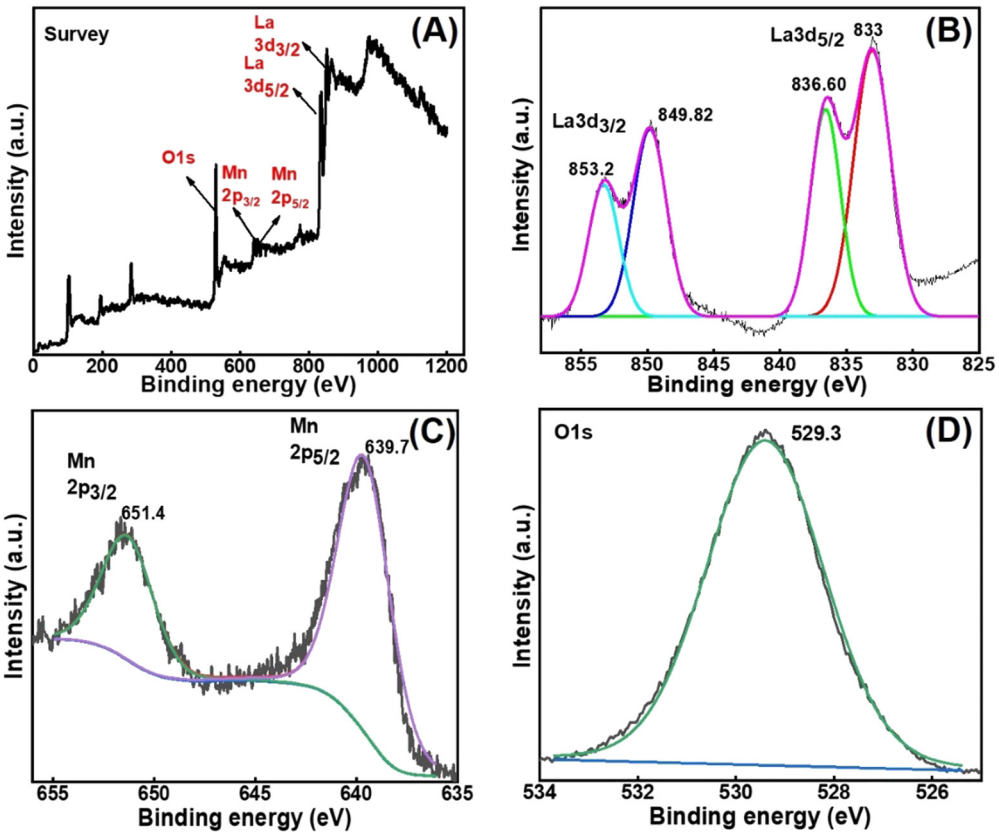

Fig. 3 (A) XPS survey spectra of rare phase nanostructure $LaMn_2O_5$. (B)–(D) XPS core level spectra of individual compounds of La 3d, Mn 2p and O 1s, respectively.

Table 1 Rms-R_q, R_a and maximum area peak height values for $LaMn_2O_5$/ITO and Tyr/$LaMnO_5$/ITO bioelectrodes

	Rms-R_q (nm)	R_a (nm)	Max. area peak height (nm)
$LaMn_2O_5$/ITO	4.39	3.39	19.65
Tyr/$LaMnO_5$/ITO	0.336	0.260	1.70

EDX mapping and consisted of lanthanum, manganese, oxygen and carbon where lanthanum and oxygen were found at 24.70 and 8.13 weight percent (Fig. 5(C)). The average particle size was 50 nm which was calculated from the TEM micrograph using ImageJ software (Fig. 5(D)).

Transmittance electron microscopy (TEM) also revealed the morphology of the materials analyzed (FEI Company of USA (S.E.A.) PTE, LTD, model name: Tecnai G220 TWIN). In the TEM image, spherical morphology appeared at scales of 100 and 50 nm, as shown in Fig. 5(E and F). From the TEM images it was also observed that the lanthanum and manganese particles were intermixed with each other in such a way as to form uniformly distributed arrangements. The HR-TEM images in Fig. 5(G) show the fringes corresponding to the (211) *hkl* plane and the SAED pattern in Fig. 5H shows the crystalline nature of the compound, with a *d*-spacing of 3.0 Å, which is also associated with the (211) plane corresponding to powder XRD data.

4. Electrochemical study

4.1. pH optimization

The appropriate current response for cyclic voltammety (CV) can be obtained at a specific pH for a particular compound. The graph of the pH study is shown between the oxidative peak current (I_{pa}) *vs.* pH and potential *vs.* pH in Fig. 6(A). To analyse the optimum pH, the CV response of the Tyr/$LaMn_2O_5$/ITO bioelectrode was optimized at various pH values (5.7–8.0). The optimum I_{pa} value was found to be 0.8273 mA at pH 6.5, which was obtained in a 50 mM phosphate buffer saline (PBS) solution with 0.9% NaCl and 5 mM $[Fe(CN)_6]^{3-/4-}$, and the scan rate was 50 mV s^{-1}. The pH graph reveals that the optimum and minimum I_{pa} values at pH 6.5 and 7.5 were found to be 0.8273 and 0.7170 mA respectively. It is clear from the pH graph that the I_{pa} values and their corresponding potentials were observed selectively at pH values 5.7, 6.0, 6.5, 7.0, 7.5, and 8.0. Moreover, the I_{pa} response was found to be maximum at pH 6.5, and therefore, this pH was used throughout the experiments.

4.2. Cyclic voltammetric (CV) study

CV was performed for the rare phase Tyr/$LaMn_2O_5$/ITO bioelectrode for the electrochemical estimation of the prepared electrode as compared to the bare electrode. The I_{pa} value for bare ITO was taken as a reference and was 0.8382 mA, considered as 100%; the I_{pa} for the $LaMnO_5$/ITO bioelectrode was 0.9098 mA, which was

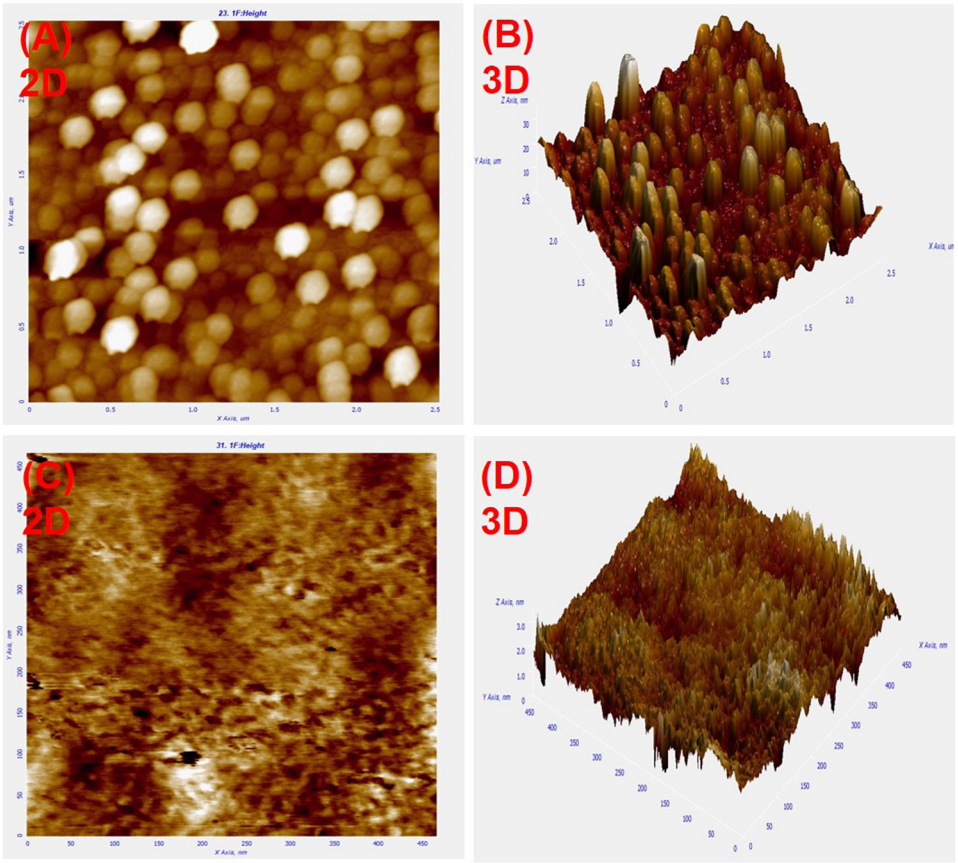

Fig. 4 (A) and (B) 2D and 3D images of AFM for the rare phase nanostructure $LaMn_2O_5$/ITO electrode. (C) and (D) 2D and and 3D images of Tyr/$LaMn_2O_5$/ITO bioelectrodes.

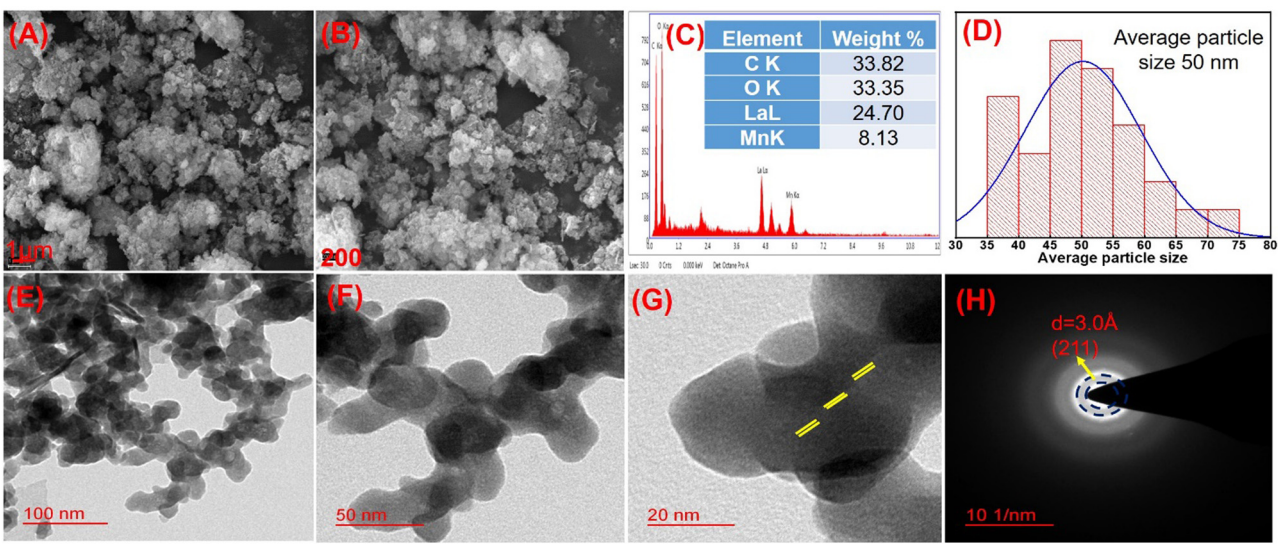

Fig. 5 (A) and (B) SEM images obtained at 1 μM and 200 nm. (C) Elemental composition present in the compound, and (D) the average particle size obtained from ImageJ software, for the prepared rare phase nanostructure $LaMn_2O_5$. (E) and (F) TEM images of $LaMn_2O_5$ at different magnifications, (G) HR-TEM image showing *d*-spacing of the prepared rare phase nanostructure $LaMn_2O_5$ and (H) SAED images showing the crystalline nature of the prepared compound.

found to be 8.54% higher than that of bare ITO. However, after immobilization of the tyrosinase enzyme, the I_{pa} increased to 0.9794 mA which was found to be 16.84% higher as compared to bare ITO (Fig. 6(B)). The differential pulse voltammetry response of the electrodes demonstrated similar findings in PBS solution compared to CV (Fig. S1, ESI†).

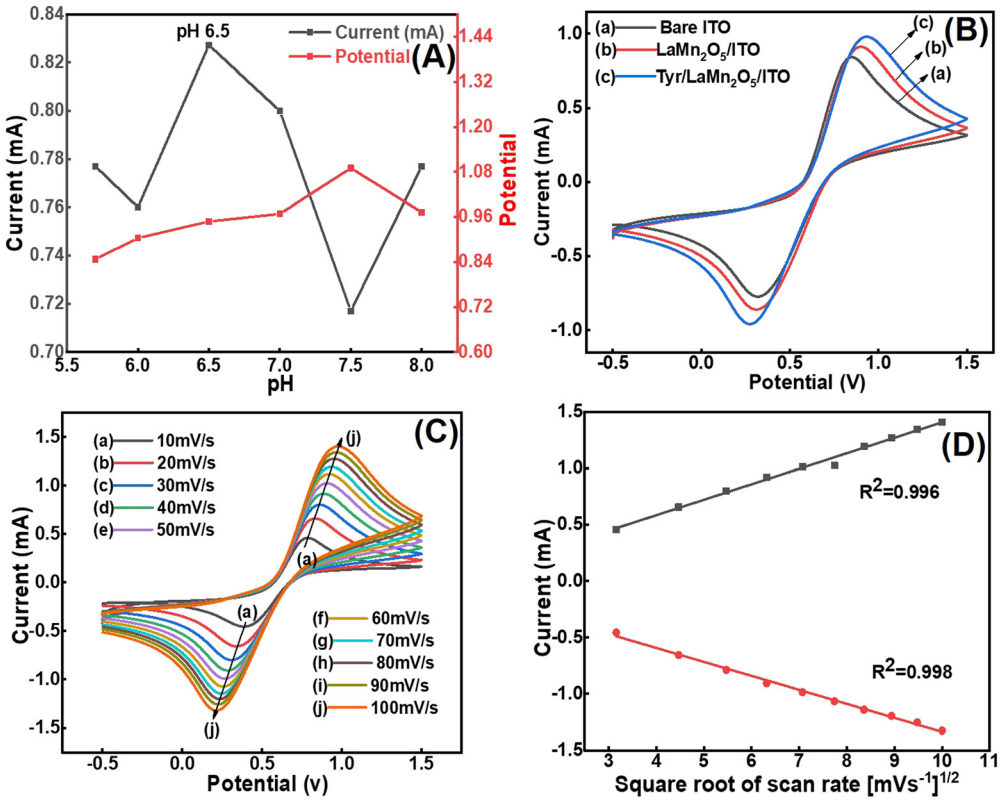

Fig. 6 (A) CV of the pH study for the Tyr/$LaMn_2O_5$/ITO bioelectrode. (B) CV of the bare ITO (a), $LaMn_2O_5$/ITO electrode (b) and Tyr/$LaMn_2O_5$/ITO bioelectrode (c). (C) The scan rate of the Tyr/$LaMn_2O_5$/ITO bioelectrode from 10 to 100 mV s^{-1}. (D) Calibration curve of the scan rate study.

The CV study reveals that as the complexity of the electrodes increases a slight increase in the potential compared to ITO was observed. This shift is due to the slight hindrance between the electrode and $[Fe(CN)_6]^{3-/4-}$.[27] The two important factors responsible for producing electrical conductivity are enzymatic and metallic behaviour. The Cu metal of the tyrosinase enzyme functions as a catalyst and increases the oxido-reductive process during the reaction where the active centre of the dinuclear copper present in the tyrosinase enzyme catalyses the conversion of phenol to orthoquinone.[28]

4.3. Scan rate and kinetics study

The rare phase nanostructure $LaMn_2O_5$ was used to analyze interfacial kinetics at different scan rates varying from 10 to 100 mV s^{-1} with the prepared Tyr/$LaMn_2O_5$/ITO bioelectrode (Fig. 6(C)). The linearly increasing and decreasing patterns of I_{pa} and I_{pc} values were obtained by increasing the scan rate. Further, the study reveals that the shift in the I_{pa} value towards a more positive and I_{pc} towards a more negative value was observed, which is suggested to be a quasi-reversible process in the redox behaviour. Moreover, from the plot of the current *vs.* square root of the scan rate [mV $s^{-1}]^{1/2}$, Fig. 6(D), an apparent linear increment in the I_{pa} and I_{pc} values was observed with a linear regression coefficient (R^2) value of 0.99 for both the anodic and cathodic peaks respectively.

Moreover, the charge transfer rate constant (K_s) value obtained by the surface modification of the prepared rare phase Tyr/$LaMn_2O_5$/ITO bioelectrode was calculated using eqn (3),

$$K_s = mnF\nu/RT \quad (3)$$

where F is the Faraday constant (96 485 C mol^{-1}); R is the gas constant (8.314 J $mol^{-1}K^{-1}$); m is the separation of the peak-to-peak (V); n =1 is the number of electrons transferred during the reaction 1; T is the room temperature (300 K); and ν is the scan rate (50 mV s^{-1}). K_s was found to be 1.23 s^{-1}, which shows the appreciable catalytic activity of the prepared materials. The potential shift [($\Delta E_p = E_{pa}$(anodic peak) − E_{pc}(cathodic peak))] value provided the linear relationship obtained with respect to the scan rate and shows that the reaction performed between the tyrosinase and Tyr/$LaMn_2O_5$/ITO electrode was a diffusion-controlled process. Further, the value of the diffusion coefficient was found for the Tyr/$LaMn_2O_5$/ITO bioelectrode applying the Randles–Sevcik equation (eqn (4)):

$$I_p = (2.69 \times 10^5)n^{3/2}AD^{1/2}C\nu^{1/2} \quad (4)$$

where the surface area (A) of the electrode is 0.25 cm^2, the number of electrons (n) is 1, I_p denotes the electrode peak current, and the concentration (C) is 5 mM at the surface. Applying these values in eqn (4), the value of D was calculated to be 0.1663 cm^2 s^{-1}. However, the value of the surface concentration of the electrode was obtained from the Brown–Anson model (eqn (5)),

$$I_p = n^2F^2\gamma AV/4RT \quad (5)$$

where γ corresponds to the surface concentration of the electrode (mol cm^{-2}), the number of electrons (n) is 1, and T is the room temperature (in K). Thus, the surface concentration obtained from eqn (5) was 5.87 × 10^{-7} mol cm^{-2}.

4.4. Electrochemical response study of the fabricated Tyr/$LaMn_2O_5$/ITO bioelectrode for bisphenol detection

The sensing behaviour of the fabricated bioelectrode is related to its electrochemical oxidation capability with the target analyte. For this purpose, the rare earth metals lanthanum and manganese were utilized. The combination of a completely vacant f orbital containing lanthanum and a filled d orbital containing manganese provided a good electrochemical response. The inherent material properties of rare phase nanostructure $LaMn_2O_5$ provide high conductivity and the fabricated tyrosinase enzyme reinforces the electrocatalytic activity of BPA.[29]

Long-range electrochemical detection of BPA was carried out using the CV technique. The Tyr/$LaMn_2O_5$/ITO bioelectrode was analysed in a PBS solution with a scan rate of 50 mV s^{-1}. A three-sensing curve was obtained with the long-range analyte from 0.001 μM to 1000 μM (Fig. 8(A–C)). A three-calibration curve was obtained in these experiments for concentrations ranging from 0.001 μM to 1000 μM, as shown in Fig. 7(D–F). The linear regression equations are

$$I_p\ (\text{mA}) = 9.1 \times 10^{-1} + C\ (\mu\text{M}) + 0.94\ (R^2 = 0.9757)\ [0.001\text{–}0.1\ \mu\text{M}] \quad (6)$$

$$I_p\ (\text{mA}) = 1.39 \times 10^{-3} + C\ (\mu\text{M}) + 0.92\ (R^2 = 0.9923)\ [1\text{–}40\ \mu\text{M}] \quad (7)$$

$$I_p\ (\text{mA}) = 1.36 \times 10^{-4} + C\ (\mu\text{M}) + 0.92\ (R^2 = 0.9781)\ [40\text{–}1000\ \mu\text{M}] \quad (8)$$

The R^2 value of the lower concentration range was 0.9757 with a 0.5% error bar; the middle concentration range was 0.9923; and the higher concentration range was 0.9781 with a 0.8% error bar. The LOD value of the bioelectrode was obtained at 2.85 × 10^{-3} μM using the formula 3 × SD/sensitivity, where SD is the standard deviation of the calibration plot of the current vs analyte concentration and the sensitivity was obtained at 3.676 mA μM^{-1} cm^{-2}, and was highly sensitive and significant for BPA sensing. Moreover, the enzyme activity was determined from the Michaelis–Menten constant (K_m) value, which was 0.007 μM (Fig. 8), calculated from the lower concentration range graph, the plot of the concentration/current *vs.* concentration taken from the sensing study. The linear regression equation for the K_m plot is

$$I_p\ (\text{mA}) = 0.96 + C\ (\mu\text{M}) + 0.94\ (R^2 = 0.9994),\ [0.001\text{–}0.1\ \mu\text{M}] \quad (9)$$

Yasuyuki *et al.* (2018) supported the purpose of the enzyme from their work on the catalytic activity of tyrosinase enzyme, where the copper metal of the tyrosinase enzyme worked as a catalyst and was responsible for the enhanced electrooxidoreductive process. Dinuclear Cu acts as an active centre of tyrosinase enzyme and catalyses the conversion of the phenolic group to orthoquinone[30] (Fig. 8(A)). A comparison between the previously reported literature and the present work is shown in Table 2.

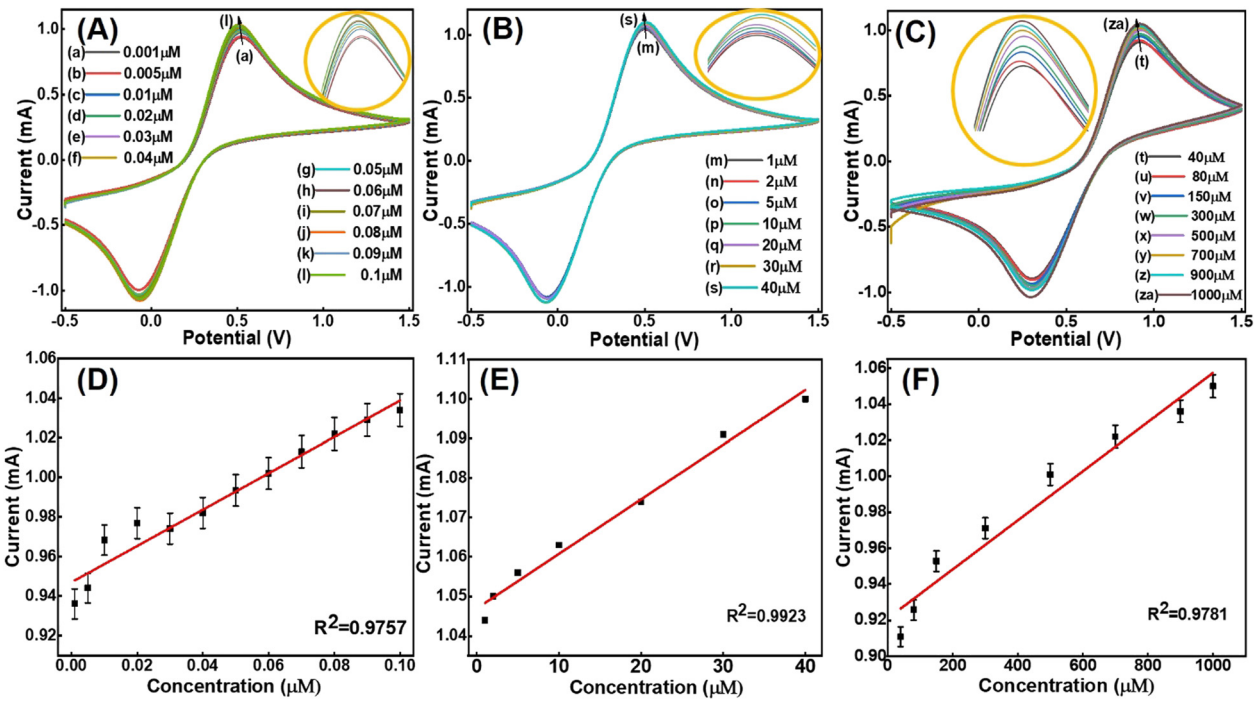

Fig. 7 (A) The CV sensing curve in the concentration range of 0.001 μM–0.1 μM, (B) the CV curve in the concentration range of 1 μM–40 μM and (C) the CV sensing curve in the concentration range of 40 μM–1000 μM, and (D)–(F) plot of the corresponding linear regression coefficients.

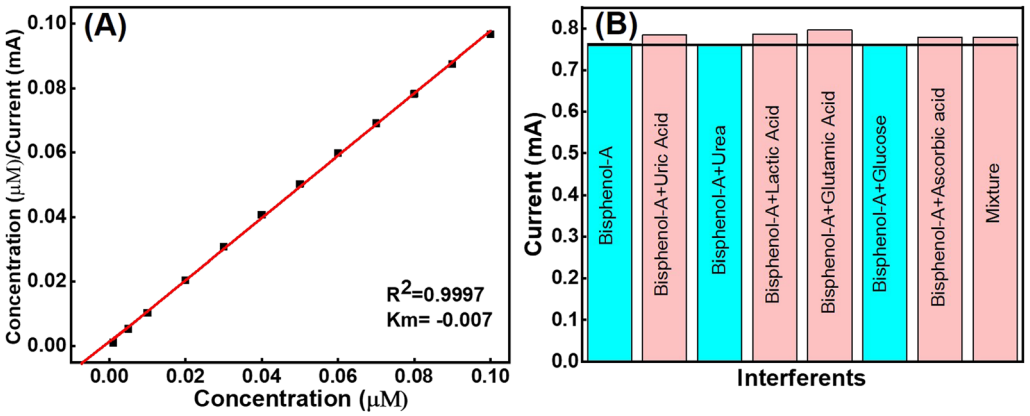

Fig. 8 (A) The Michaelis–Menton constant (K_m) determined from the plot of concentration/current *vs.* concentration obtained from the sensing study and (B) the selectivity analysis for BPA using various interference analytes.

Table 2 Comparison of the previously reported studies and the present work

S. no.	Electrode	Method	Linearity (μM)	LOD (μM)	Ref.
1	MIPs MNPs/CTAB/CPE	CV	0.6–100	0.1	31
2	GOMWCNT-βCD/SPE	LSV	0.05–30	6×10^{-3}	32
3	1T&2H-MoS_2/CNTs-NH_2	CV	0.01–70	8.6×10^{-3}	33
4	Fe–Cu-BTC/AuNPs/GCE	DPV	0.1–18	18×10^{-3}	34
5	CB/f-MWCNTs	CV	0.1–130	0.08	35
6	SWCNT/GCE	CV	10–100	7.3	36
7	NFO/SPCE	DPV	0.02–12.5	6×10^{-3}	37
8	Tyr/$LaMn_2O_5$/ITO	CV	0.001–1000	2.85×10^{-3}	Present work

4.5. Selectivity of the fabricated Tyr/$LaMn_2O_5$/ITO bioelectrode or the effect of interference

The selectivity of the rare Tyr/$LaMn_2O_5$/ITO bioelectrode was optimized to determine the effect of analytes with several interferents present in the human blood samples. For this, the CV was analyzed in the same PBS solution where uric acid (UA), urea, lactic acid (LA), glutamic acid (GA), glucose (Glu), ascorbic acid (AA) and the mixture (Mix) were taken as interferents. The study revealed that no interferents significantly interrupted the standard BPA analyte (Fig. 8(B)). The %RSD values for different analytes are shown in Table 3.

Moreover, the selectivity analysis was carried out using a phenolic group containing compounds like 2-aminophenol, 2-nitrophenol, 4-aminophenol, and hydroquinone, resorcinol (Fig. S2 in ESI†). In this experiment, the concentration of each interferent solution was 50 μM and the concentration of BPA was 100 μM. The % RSD values for different analytes are given in Table S1 (ESI†).

Table 3 %RSD values for the interferents in the selectivity analysis

BPA with interfering substance (20 μM each)	Cathodic peak current (I_p; mA)	% RSD
BPA	0.7629	Standard
BPA-UA	0.7840	2.76
BPA-urea	0.7622	−0.10
BPA-LA	0.7863	3.06
BPA-GA	0.7959	4.32
BPA-Glu	0.7616	−0.18
BPA-AA	0.7770	1.84
BPA-Mix	0.7785	2

The obtained results indicate very low to negligible interferents with various analytes because the enzyme tyrosinase provided more selectivity to the prepared compound. Thus, the prepared Tyr/$LaMn_2O_5$/ITO bioelectrode is found to be effective and selective for bisphenol-A.

4.6. Response time, reusability and stability of the fabricated Tyr/$LaMn_2O_5$/ITO bioelectrode

A response time study was carried out to determine the time period at which the electrode performed at high efficiency which was analysed from the CV measurement and experiments were performed in the PBS solution. The CV was performed from 0 to 40 second time intervals and it was observed that the oxidative current response was found to increase up to 10 seconds and then slightly decreased up to 20 seconds. However, on increasing the time interval, the optimum current was obtained at 30 seconds as shown in Fig. 9(A). Further, the current response was found to decrease with increasing time interval. Thus 30 seconds was found to be a more appropriate response time for the prepared electrode and was used throughout the experiments.

The reusability of the electrode was evaluated to determine the maximum possibility of repeating the electrode which was obtained in a similar phosphate buffer. CV was performed 16 times where at the 13th scan, the I_{pa} value was found to be optimum, considered as 100%. Further, at the 14th, 15th and

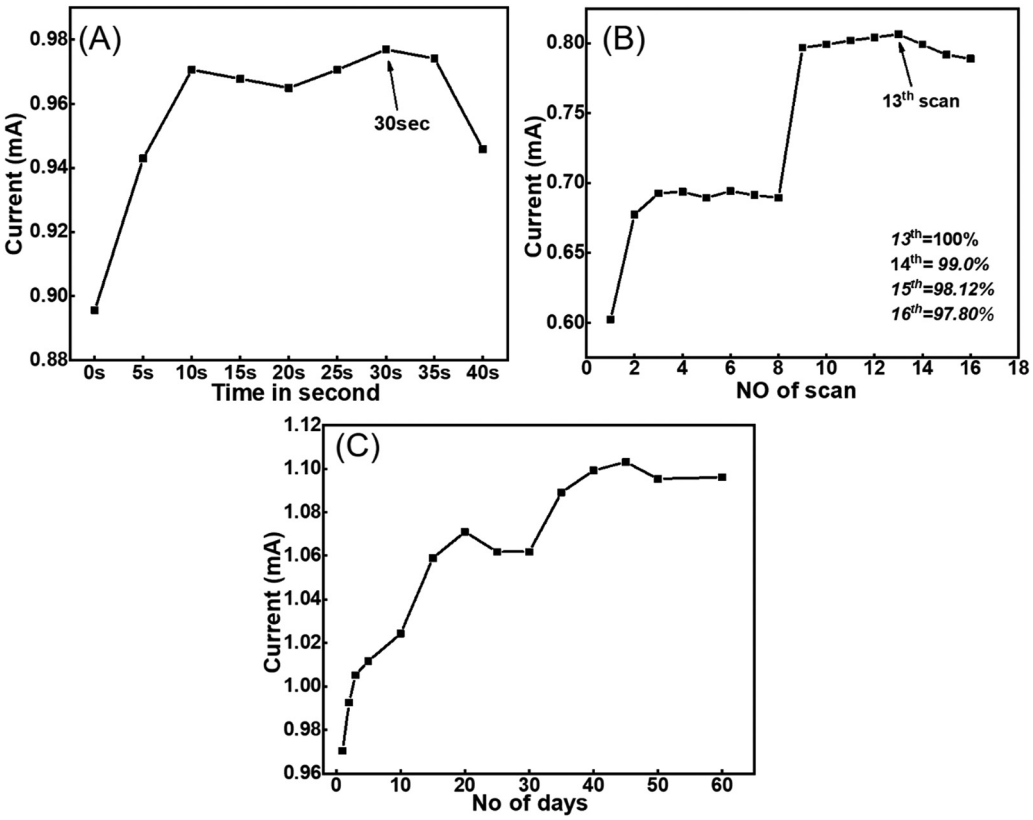

Fig. 9 (A) The response time and (B) the reusability of the prepared Tyr/$LaMn_2O_5$/ITO bioelectrode. (C) The stability graph obtained for the rare phase Tyr/$LaMn_2O_5$/ITO bioelectrode.

16^{th} scans, the I_{pa} values were found to decrease to 99.0%, 98.12% and 97.80% respectively. Thus, the reusability of the prepared electrode was 13 days (Fig. 9(B)).

The stability of the prepared electrode was determined to obtain the current response for the maximum number of days. The CV was performed in PBS solution at the same scan rate for 0 to 60 days. The anodic peak current value was found to increase up to 20 days and then decrease up to 30 days. Further, the I_{pa} value was found to increase and remained constant for up to 60 days, as shown in Fig. 9(C). Thus, the prepared electrode was stable for 60 days.

5. Conclusion

We have successfully synthesized the rare phase nanostructure $LaMn_2O_5$ using a biogenic method, with the Kachnar extract as a reducing agent. XRD provided the *hkl* values and an average crystallite size of approximately 14.45 nm. The FT-IR spectroscopy confirmed the characteristic peaks of La–O and Mn–O bonds, elemental oxidation states and electronic environments, which were further supported by XPS analysis. The optical spectra obtained were similar to those previously reported for the absorbance and emission spectra. AFM analysis revealed a uniform spherical morphology of the compounds. Morphological arrangements were obtained from SEM and TEM analyses and corresponded well with the AFM results. The HR-TEM images showed three distinct arrangements representing the different phases of the prepared compounds, as supported by the obtained fringes. The SEAD images confirmed the crystalline nature of the prepared rare phase nanostructure $LaMn_2O_5$, with an average particle size of approximately 50 nm. We also detected BPA, an endocrine disruptor, using the cyclic voltammetric method in the long concentration range of 0.001 μM to 1000 μM, spanning three distinct concentration ranges from 0.001 μM to 0.1 μM, 1.0 μM to 40 μM, and 40 μM to 1000 μM with R^2 values of 0.9757, 0.9923, and 0.9781 respectively. The compound demonstrated a sensitivity of 3.67 mA μM^{-1} cm^{-2}, and the LOD value was found to be 2.85×10^{-3} μM. The compound exhibited high selectivity for BPA with a negligible % RSD value for interferents. An excellent response time of 30 seconds was achieved, and the compound showed reusability for approximately 13 days with long-term stability for 60 days. Overall, we found that the biologically synthesized rare phase nanostructure $LaMn_2O_5$ is a good sensor for BPA detection and has great potential for device development in the future.

Author contributions

A. S.: data curation, investigation, visualization, writing – original draft. K. R. B. S.: data curation, validation, visualization, writing – original draft. J. S. and M. D. P.: conceptualization, validation,

project administration, supervision, writing – review & editing of the original draft.

Conflicts of interest

The authors declare that they have no known competing financial interests or personal relationships that could have appeared to influence the work reported in this paper.

Acknowledgements

This work received no specific grant from public, commercial, or not-for-profit funding agencies. The authors, A. S. and K. R. B. S., would like to express their gratitude to Banaras Hindu University (BHU), Varanasi, for providing the necessary facilities to conduct the research work. Additionally, the authors acknowledge the SATHI facility, located at Banaras Hindu University's CDC building, for providing XPS and TEM analysis. Furthermore, J. S. and M. D. P. would like to acknowledge BHU for providing a seed grant and incentive grant respectively under the MoE Govt India, Institute of Eminence (IoE) scheme 6031.

References

1 S. K. Ghosh, *ACS Omega*, 2020, **5**, 25493–25504.
2 G. Charalampides and K. I. Vatalis, *J. Geosci. Environ. Prot.*, 2015, **03**, 66–73.
3 M. Mauri, V. Collico, L. Morelli, P. Das, I. García, J. Penaranda Avila, M. Bellini, R. Rotem, M. Truffi, F. Corsi, R. Simonutti, L. M. Liz-Marzán, M. Colombo and D. Prosperi, *ACS Appl. Nano Mater.*, 2020, **3**, 3787–3797.
4 Y.-H. Son, P. T. M. Bui, H.-R. Lee, M. S. Akhtar, D. K. Shah and O.-B. Yang, *Coatings*, 2019, **9**, 631.
5 Q. He, G. Li, X. Liu, J. Liu, P. Deng and D. Chen, *Catalysts*, 2018, **8**, 323.
6 C. M. Julien and A. Mauger, *Nanomaterials*, 2017, **7**, 396.
7 A. Srivastava, G. Mishra, K. R. Singh, J. Singh, R. Pandey and M. D. Pandey, *Luminescence*, 2023, **38**(7), 1347–1357.
8 A. Srivastava, G. Mishra, J. Singh and M. D. Pandey, *Mater. Lett.*, 2022, **308**, 131231.
9 J. Ji, Z. Cai and L. Shen, *Fuel*, 2024, **357**, 129974.
10 J. A. Chavarría-Rubio, D. A. Cortés-Hernández, A. M. Garay-Tapia and G. F. Hurtado-López, *J. Magn. Magn. Mater.*, 2022, **553**, 169253.
11 T. Chen, X. Wang, S. Ma, X. Ma, Y. Zhang, L. Luo and Z. Yuan, *Solid State Sci.*, 2020, **108**, 106425.
12 Z. Y. Zhao, M. F. Liu, X. Li, L. Lin, Z. B. Yan, S. Dong and J.-M. Liu, *Sci. Rep.*, 2014, **4**, 3984.
13 W. Peng, V. Balédent, M.-B. Lepetit, A. Vaunat, E. Rebolini, M. Greenblatt and P. Foury-Leylekian, *Acta Crystallogr., Sect. B: Struct. Sci., Cryst. Eng. Mater.*, 2019, **75**, 687–696.
14 Y. Chen, H. Yuan, G. Tian, G. Zhang and S. Feng, *J. Solid State Chem.*, 2007, **180**, 1340–1346.
15 L. Ming, L. Song, J. Xu, R. Wang, J. Shi, M. Chen and Y. Zhang, *ACS Appl. Mater. Interfaces*, 2021, **13**, 35444–35455.
16 S. Ahmed, M. Ahmad, B. L. Swami and S. Ikram, *J. Adv. Res.*, 2016, **7**, 17–28.
17 A. K. Sidhu, N. Verma and P. Kaushal, *Front. Nanotechnol.*, 2022, **3**, 801620.
18 D. Sahoo, A. Ahmad, J. Ahmad and S. Tandon, *J. Essent. Oil Bear. Plants*, 2013, **16**, 636–640.
19 L. N. Vandenberg, M. V. Maffini, C. Sonnenschein, B. S. Rubin and A. M. Soto, *Endocr. Rev.*, 2009, **30**, 75–95.
20 Z. Chen, R.-J. Xiao, C. Ma, Y.-B. Qin, H.-L. Shi, Z.-W. Wang, Y.-J. Song, Z. Wang, H.-F. Tian, H.-X. Yang and J.-Q. Li, *Front. Phys.*, 2012, **7**, 429–434.
21 J. Singh, K. R. Singh, M. Kumar, R. Verma, R. Verma, P. Malik, S. Srivastava, R. P. Singh and D. Kumar, *Mater. Adv.*, 2021, **2**, 6665–6675.
22 A. K. M. A. Ullah, M. M. Haque, M. Akter, A. Hossain, A. N. Tamanna, M. M. Hosen, A. K. M. F. Kibria, M. N. I. Khan and M. K. A. Khan, *Mater. Res. Express*, 2020, **7**, 015088.
23 M. Ghiasi and A. Malekzadeh, *Superlattices Microstruct.*, 2015, **77**, 295–304.
24 S. Wu, M. Xie, Q. Zhang, L. Zhong, M. Chen and Z. Huang, *Molecules*, 2017, **22**, 1117.
25 J. Zhou, L. Shi, Q. Liu, H. Zhang, X. Liu, F. Han, Z. Guo, X. Lu and J. Wang, *Part. Part. Syst. Charact.*, 2020, **37**, 2000143.
26 X. Huang, P. Niu, M. Li, H. Liao and X. Shang, *J. Wuhan Univ. Technol. Sci. Ed.*, 2018, **33**, 23–29.
27 N. Jaiswal, C. M. Pandey, A. Soni, I. Tiwari, M. Rosillo-Lopez, C. G. Salzmann, B. D. Malhotra and G. Sumana, *Sens. Actuators, B*, 2018, **275**, 312–321.
28 F. Ye, C. Feng, N. Fu, H. Wu, J. Jiang and S. Han, *Appl. Surf. Sci.*, 2015, **357**, 1251–1259.
29 A. Alsbaiee, B. J. Smith, L. Xiao, Y. Ling, D. E. Helbling and W. R. Dichtel, *Nature*, 2016, **529**, 190–194.
30 Y. Matoba, S. Kihara, N. Bando, H. Yoshitsu, M. Sakaguchi, K. Kayama, S. Yanagisawa, T. Ogura and M. Sugiyama, *PLoS Biol.*, 2018, **16**, e3000077.
31 L. Zhu, Y. Cao and G. Cao, *Biosens. Bioelectron.*, 2014, **54**, 258–261.
32 A. U. Alam and M. J. Deen, *Anal. Chem.*, 2020, **92**, 5532–5539.
33 L. Zhang, H. Tao, C. Ji, Q. Wu, X. Wang and Y. Wu, *New J. Chem.*, 2022, **46**, 8203–8214.
34 M. B. Nguyen, N. H. Anh, V. Thi Thu, P. Thi Hai Yen, P. Hong Phong, L. Quoc Hung, N. T. T. Ngan, T. Q. Hai and V. Thi Thu Ha, *RSC Adv.*, 2022, **12**, 33825–33834.
35 A. Thamilselvan, V. Rajagopal and V. Suryanarayanan, *J. Alloys Compd.*, 2019, **786**, 698–706.
36 P. Kanagavalli and S. Senthil Kumar, *Electroanalysis*, 2018, **30**, 445–452.
37 G. Kesavan, N. Nataraj, S.-M. Chen and L.-H. Lin, *New J. Chem.*, 2020, **44**, 7698–7707.

